THE JOURNAL OF PHYSICAL CHEMISTRY Letters

Letter

pubs.acs.org/JPCL

Nanopore-Based Sensors for Ligand–Receptor Lead Optimization

Binquan Luan,* Tien Huynh, and Ruhong Zhou*

Computational Biology Center, IBM Thomas J. Watson Research, Yorktown Heights, New York 10598, United States

Supporting Information

ABSTRACT: Developing a low-cost and high-efficacy method to optimize prescreened or designed drug candidates will facilitate drug discovery and biomedical research in general. Current methods of drug screening usually involve tedious sample preparation and costly biological/chemical assays. Here, through all-atom molecular dynamics simulations, we propose a new drug optimization method, based on the nanopore force spectroscopy, to electrically detect the binding strength between a drug molecule and a target protein. Simulation results demonstrate that the drug–protein complex can be electrophoretically driven into a nanopore, which is followed by the rupture of the complex at a critical biasing voltage. The latter determines the binding strength of the tested drug molecule. It is expected that the application of this single-molecule technology could help to accelerate the drug discovery, particularly for processes of the narrow screening and further lead optimization.

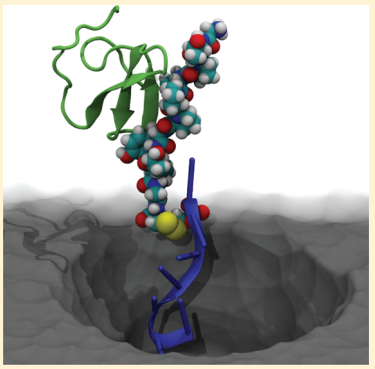

Recent advances in the high-throughput screening (HTS) methods[1] enable the screening of hundreds of thousands of compounds per day, giving new promises to the discovery of pharmaceutical drug candidates. From the HTS, active compounds with the potential of inhibiting or activating functions of a target biomolecule (such as an enzyme) are identified for subsequent lead optimization. Although additional designed compounds, according to common structural features of prescreened ones, are often further produced during the lead optimization process, the total number of drug candidates is usually limited. Thus, for the lead optimization, the accuracy in optimizing a drug molecule that can selectively bind to a target protein is more important than the speed. Therefore, a deep understanding of the molecular recognition/binding processes of small ligands by protein receptors is crucial for the design of new drugs in pharmaceutical research. However, despite extensive studies in the last few decades, an accurate, fast, and reliable measurement for ligand–receptor binding affinity, or dissociation constant (K_d), is still largely nonexistent, particularly for those high-affinity ligands (those subnanomolar ligands).[2]

More generally, there is a growing interest in investigating the nature of molecular recognition (binding) processes between biomolecules because these specific interactions regulate the essential processes (such as metabolism) of life. Namely, there are three fundamental approaches in terms of receptor binding experiments that are based on kinetic, saturation, or competition/modulation experiments.[2] Many techniques have been developed over the years for these approaches, with a few representative ones described below. The traditional fluorescence spectroscopy and isothermal titration calorimetry (ITC) can measure the binding affinity through titration (or displacement titration for higher affinity binders, where two titrations are carried out: a direct titration of the weak ligand to the target macromolecule and a displacement titration of the high-affinity ligand to the weak ligand–target complex).[3,4] In fluorescence spectroscopy, either the potent or the weak ligand has a fluorescent label exhibiting different intensities for bound and free states. In the case of ITC, unlike the fluorescence spectroscopy, there is no need for labels, but the enthalpy of binding for both ligands must be significantly different.[3,4] One can also use differential scanning calorimetry (DSC) for binding affinity measurement. When a ligand interacts preferentially with the native state of a protein, it stabilizes the protein against thermal denaturation. From the increase of the stability, it is possible to estimate the binding affinity.[5] Although this methodology allows determination of strong affinities, it is somewhat imprecise because one must extrapolate in temperature in order to calculate the binding affinity at lower temperature.[5] In addition, surface plasmon resonance (SPR) was also proposed to determine K_d's in the subnanomolar range. The main advantage is the ability to study molecular interactions in a label-free setting, but the problem with using a concentration at or below the affinity for subnanomolar interactions is the time for equilibrium (it can be days or even weeks); thus, any end-point assay must be incubated properly to guarantee accurate results.[6,7] Recently, nuclear magnetic resonance (NMR) spectroscopy (the so-called saturation transfer difference (STD) NMR) was also used to investigate the ligand–receptor binding; however, a direct evaluation of K_d from the variation of STD NMR values is still not feasible due to the complex dependence of STD intensities on the spectral properties of the observed signals.[8] Therefore, new techniques, particularly the single-molecule-based techniques, that can supplement these elegant yet not

Received: December 4, 2014
Accepted: January 6, 2015

DOI: 10.1021/jz5025614
J. Phys. Chem. Lett. 2015, 6, 331–337

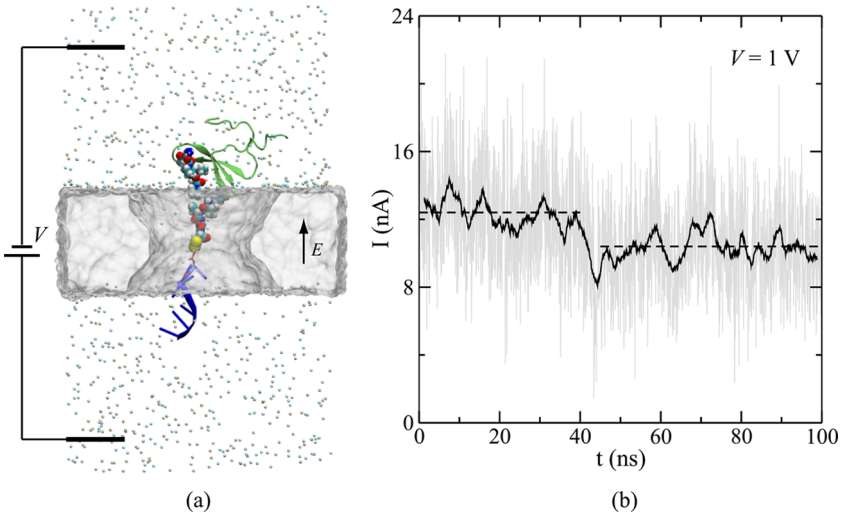

Figure 1. Illustration of the nanopore-based drug-screening sensor. (a) Simulation system: the hourglass-shaped nanopore is shown transparently; atoms in the drug-like molecule are shown as van der Waals spheres; the linker is highlighted in yellow; the ssDNA fragment is shown in blue; the target protein is in cartoon representation; potassium and chlorine ions are respectively shown as tan and cyan dots; water molecules are not shown. (b) Simulated ion current recording during the transport of the complex. The biasing voltage is 1 V.

perfect ones are still in great demand for this important and challenging problem.

Here, we propose a physical method based on the nanopore sensor to electrically detect the binding between a drug candidate and a target protein. Emerging from the idea of a membrane protein channel for transporting molecules (such as ssDNA),[9] solid-state nanopores with nanometer-sized holes spanning a thin solid membrane have been extensively studied as a biological sensor.[10−12] When a single biological molecule is forced into a nanopore, its physical information (such as the size and charge) can be inferred from the signals of ion currents through the pore. For example, a solid-state-nanopore-based device has been proposed as the platform for next-generation DNA sequencing[10] and protein analyses.[13,14] Equally important, the so-called "nanopore force spectroscopy (NFS)", a nanopore-based device, has been applied to detect the mechanical rupture force in a complex.[15]

The principle of the NFS was first demonstrated in analyzing the DNA−protein interaction using a single α-hemolysin nanopore.[15] When the charged DNA molecule is electrophoretically driven through the nanopore by a biasing voltage across the lipid membrane, a bound protein on the DNA is too large to enter the pore and is therefore blocked at the entrance. After ramping up the biasing voltage, the effective electric driving force on the DNA gradually increases. Consequently, the (binding) energy profile is tilted, yielding a reduced energy barrier for disassociation. Eventually, a rupture between the DNA and protein molecules occurs at a critical biasing voltage, when the thermal fluctuation is enough to overcome the reduced energy barrier. Recently, the NFS has also been applied for a solid-state nanopore. For example, the single nucleotide polymorphism (SNP) in the complex of the DNA and the restriction enzyme could be detected by a synthetic nanopore;[16] the single-molecule bond between the biotin and the neutravidin was characterized by a solid-state NFS.[17]

Similarly, it may be possible to utilize the NFS to test the binding between a drug candidate and a target protein. Using all-atom molecule dynamics (MD) simulations, we theoretically investigated the feasibility of using the NFS in the lead optimization of drug candidates. As a proof-of-principle study, we simulated the transport and rupture of a complex including a drug-like molecule and a target protein. Figure S1 (Supporting Information) shows an example of a prepared complex for the NFS-based drug testing. Similar to the drug molecule inhibiting a protein enzyme, the GTPPPPYTVGC peptide (the drug-like molecule) binds the WW domain (the target protein) in the complex. In order to electrophoretically drive the complex of the drug-like molecule and the target protein toward the nanopore sensor, one end of the peptide is functionalized with a ssDNA fragment. The linker (connecting the peptide and the ssDNA) contains a disulfide bond, namely, $-CH_2-S-S-CH_2-$, formed from the oxidization of the thiolated C terminal (cytosine) of the peptide and the thiolated 3′ end of the ssDNA. Experimentally, it has been shown previously that an α-hemolysin pore whose N-terminal has similar functionalization was electrically driven into a solid-state nanopore.[18]

We adopted the all-atom MD method, which is widely used in the studies of both biomolecules[19−22] and novel nanotechnologies,[23−26] to demonstrate the transport and rupture processes of the complex in a nanopore. The simulation system is illustrated in Figure 1a. The 30-Å-in-thickness membrane, made of an amorphous SiO_2 solid, separates the cis and trans fluidic chambers. An hourglass-shaped nanopore was "drilled" through the membrane. Radii of the pore "neck" and the pore opening were 15 and 25 Å, correspondingly. The solid-state nanopore was then solvated by a 1 M KCl electrolyte. We adopted the atomic structure of the protein−ligand complex (PDB ID: 1JMQ) in which a proline-rich ligand is bound to the active site of the WW domain. One end of the ligand was then further "linked" (via the disulfide bond) to a ssDNA fragment ($Poly(dA)_7$), as shown in Figure S1 (Supporting Information). The total charge Q of the ssDNA fragment was $7e$, where e is the charge of an electron. Note that the exact number of charges in the ssDNA (or the ssDNA length) can be arbitrary. Initially, the free end of the ssDNA was close to the entrance of the nanopore, while the center of mass (COM) of the target protein was about 58 Å above the pore. A biasing electric field, perpendicular to the membrane surface, was applied in simulations to drive the charged complex towards the

DOI: 10.1021/jz5025614
J. Phys. Chem. Lett. 2015, 6, 331−337

nanopore. Experimentally, the biasing electric field was applied across the membrane by inserting two electrodes (such as Ag/AgCl electrodes connected to a battery) into the cis and trans chambers, respectively.

All simulations were carried out using specially optimized NAMD2.9[27] on the IBM Bluegene Supercomputer. First, the entire simulated system was equilibrated at 1 bar and 300 K for 5 ns. During the equilibration, non-hydrogen atoms in the complex were harmonically restrained. The equilibrated system measured 81 × 81 × 142.2 Å^3. Subsequent simulations, with applied biasing voltages, were carried out in the *NVT* ensemble. Atoms in the solid membrane were harmonically restrained to their original positions to prevent the solid membrane from moving during simulations. The Langevin dynamics was applied to all atoms in the solid membrane to maintain a constant temperature (300 K) in the simulated system. We applied the TIP3P model[28,29] for water and a standard ion force field[30] and silica force field for the solid membrane.[31] The CHARMM force field[32] was used for the modeled ssDNA and protein. A smooth cutoff (10−12 Å) was used to calculate van der Waals energies. Electrostatic interactions were calculated using the particle-mesh Ewald (PME) method (grid size ≈ 1 Å). The integration time step in all production MD simulations was 1 fs.

In a biasing electric field, the charged complex is electrically driven into the nanopore, as shown in Figure 1a. In order to trap the protein molecule during the translocation process at the entrance of the nanopore, it is important to make the size of the nanopore larger than both the ssDNA and drug-like molecule but smaller than the target protein. When the biasing voltage (such as 1 V) is not large enough to pull the complex apart, the entire complex is trapped at the nanopore entrance. This translocation process can be monitored by measuring the ion current through the nanopore. After the complex is trapped at the nanopore, the pore current is reduced from the open-pore value (12.3 nA, in this case) to the blockage one (10.3 nA), caused by the partial blockage of the nanopore by the complex. The open-pore current is consistent with the value from our previous study.[33] When the biasing voltage is increased to 2 V, the ssDNA along with the linked drug-like molecule is further driven through the nanopore, indicating that the electric driving force exceeds the rupture force needed to pull the drug-like molecule away from the target protein.

Figure 2a−d illustrates the entire process for the NFS to characterize the binding between the drug-like molecule and target protein. Figure 2e shows the time-dependent COM of the drug-like molecule when transiting the nanopore at various biasing voltages. When V_{bias} = 1 V, the COMs (z-component) of the drug-like molecule fluctuate before the entry of the complex into the pore (Figure 2a), indicating the diffusive motion. This is because the biasing voltage mainly drops at the pore region (see below). At around 45 ns, Figure 2e shows that the COMs drop suddenly and become constant thereafter, corresponding to the capture (Figure 2b) and the trapping (Figure 2c) of the complex, respectively. During the remaining 50 ns simulation after the complex being trapped, no rupture between the drug-like molecule and target protein occurs. Correspondingly, the pore current is kept at the blockage level (Figure 1b). When increasing the biasing voltage to 1.5 V after the trapping, there is still no rupture event (purple line in Figure 2e), indicating the electric driving force is still not large enough for the rupture to occur. Consistently, when lowering the biasing voltage to 0.5 V after the trapping, as expected,

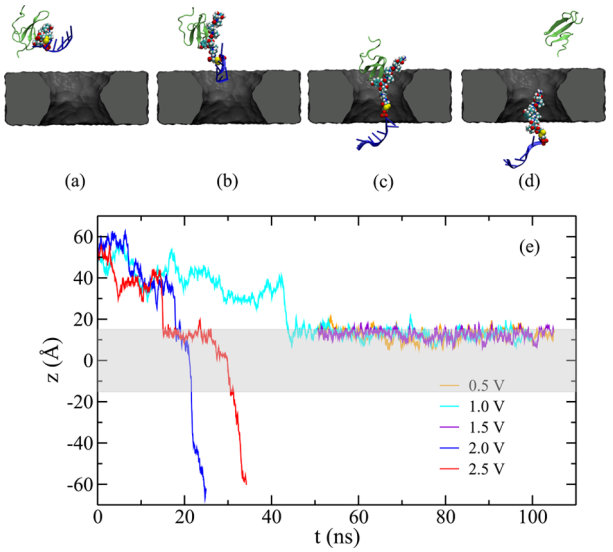

Figure 2. Transport process of the complex through the nanopore at various biasing voltages. (a−d) Snapshots of the transport process when V_{bias} is 1 V (a−c) and 2 V (d). (e) The time-dependent COMs of the drug-like molecule when V_{bias} = 0.5 (orange), 1.0 (cyan), 1.5 (purple), 2.0 (blue), and 2.5 (red) V. The shaded area shows where the nanopore is (−15 < z < 15 Å).

there is also no rupture event (orange line in Figure 2e). In these cases, the pore current remains at the blockage level for each biasing voltage.

After further increasing the biasing voltage to 2.0 V, Figure 2e (red line) shows that the COMs of the drug-like molecule continue decreasing after the complex being trapped by the nanopore, indicating that the rupture between the drug-like molecule and target protein has occurred (as shown in Figure 2d). At even higher biasing voltage (2.5 V), the rupture event occurs consistently (blue line in Figure 2e), as expected. In experiment, a rupture event is signified by an increase of the ion current to the open-pore value. Therefore, the critical voltage V_{cr} that is required for electrically pulling the drug-like molecule apart from its bound protein is about 2.0 V in this case.

By monitoring the transport process (via the pore current), it is possible to determine the critical biasing voltage at which the rupture occurs. The rupture force can be estimated using $q_{eff}V_{cr}/D$, where q_{eff} is the effective charge of the drug−ssDNA fragment (inside of the pore) after the ionic screening in an electrolyte and D is the thickness of a solid-state membrane. Additionally, the interaction strength (thus the binding affinity) between a tested drug-like molecule and the target protein can be estimated from V_{cr} (see below).

To show details in the ligand−receptor interaction during the transport and rupture processes, we identified non-hydrogen atoms in the target protein that are in contact with the ligand (drug-like molecule) for each simulation trajectory. Here, a protein atom is considered to be in contact with the drug-like molecule if it is within 3 Å of that molecule. Figure 3 shows the number of these atoms versus the z-component of the COMs of the drug-like molecule in each simulation trajectory. All simulations were started with the complex being at least 58 Å above the pore. When V_{bias} = 1.0 V, the simulation result shows that the complex was driven into the pore and subsequently trapped inside of it (see the dense points around the pore entrance; Figure 3a). For the slightly larger V_{bias} (1.5 V) or even the smaller one (0.5 V), the position-dependent drug−protein

DOI: 10.1021/jz5025614
J. Phys. Chem. Lett. 2015, 6, 331−337

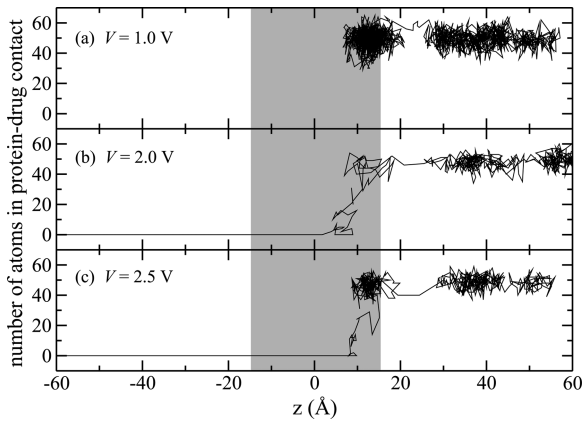

Figure 3. Number of non-hydrogen atoms in the drug-like molecule that are in contact with the target protein during translocation processes at different voltages: (a) 1.0; (b) 2.0; and (d) 2.5 V. Each set of data points is taken from the simulation trajectory every 50 ps. The shaded area shows where the nanopore is located.

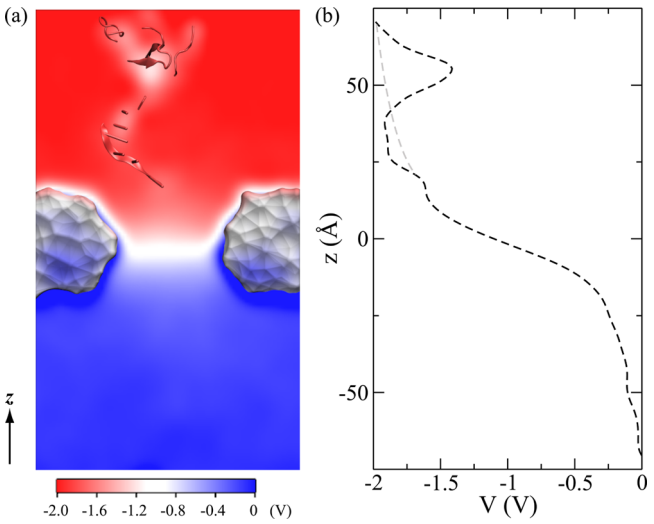

Figure 4. Distribution of electric potentials in simulated systems with a biasing voltage of 2.0 V. (a) Two-dimensional map of electric potentials on the y = 0 plane. (b) Potentials along the z-axis that coincide with the symmetry axis of the pore. The potential fluctuation in the $z > 0$ region is due to the presence of the complex. The gray dashed line illustrates the potential distribution without the presence of the complex.

contacts are similar. Notably, when the z-components of the COMs (of the drug-like molecule) are around 25 Å, fast directional motion (toward the pore) of the molecule, reflected by much more sparse points in Figure 3a, replaced the mostly diffusive motion when the complex was further away from the pore. This is related to the ssDNA capture (by the pore) followed by the electrophoretic transport of the ssDNA through the pore. This indicates that the biasing electric field is stronger near the pore region than far away from the pore, which is confirmed in analyses of the field distribution below. Thus, the drug-like molecule was dragged by the ssDNA toward the pore. The same transport behavior near the pore entrance can be discerned for the cases when V_{bias} = 2.0 and 2.5 V (see Figure 3b and c).

Because of the finite binding energy between the drug-like molecule and the target protein, the applied V_{bias} on average should be larger than V_{cr} before the drug-like molecule can be pulled through the pore. As shown in two simulations (Figure 3b and c), the drug-like molecule was pulled through the nanopore when V_{bias} = 2.0 or 2.5 V. After that, the target protein and the drug-like molecule were respectively in the cis and trans chambers. Accordingly, the number of contacting atoms is zero (Figure 3b and c).

To estimate the rupture force, we need to extract the distribution of electrostatic potentials in the simulated system. The Poisson equation was used to solve the potentials,[34] given the atomic positions and charges averaged over 50 ns of simulation in which the complex was restrained above the nanopore. Figure 4a shows the two-dimensional map of electrostatic potentials on the plane (x=0) when V_{bias} = 2 V. Potentials are nearly constant (i.e., nearly uniform color in Figure 4a) when far away from pore openings and change sharply inside of the pore. Figure 4b shows potentials on the z-axis (that is also the symmetry axis of the pore). Because the ssDNA fragment is negatively charged ($7e$ in this case) and the target protein is positively charged ($-1e$), potentials near the complex are correspondingly modified. As discussed above, the biasing voltage mainly drops near and inside of the pore ($-15 < z < 15$ Å).

Theoretically, because of the current conservation, the ion current inside of the nanopore is same as the ones outside of the pore. Assuming that ion concentrations and mobilities are constant (which is approximately true for 1 M KCl electrolyte and the neutral pore), the current conservation yields the relation $E_pS_p = E_cS_c$, where E_p and E_c are electric fields inside and outside of the pore respectively; S_p and S_c are cross-sectional areas of the nanopore and the chamber, respectively. Because the cross-sectional area of the nanopore is much smaller than that of the cis or trans chamber, the electric field E_p inside of the nanopore is much larger than the electric field E_c outside of the pore. Therefore, the slope of dV/dz (or the electric field) is much larger inside of the pore than outside of the pore, as shown in Figure 4b.

From the simulation trajectory (V_{bias} = 2 V), we calculated the number of counterions (K^+) N within 3 Å (the rough Debye length for ionic screening in a 1 M KCl electrolyte) of the drug−ssDNA fragment inside of the nanopore. Thus, without taking into account the hydrodynamic screening of ssDNA,[35] the effective charge of the fragment $q_{eff} = Q - N$, where Q is the total charge of the bare drug−ssDNA fragment inside of the nanopore. The time-dependent q_{eff}, obtained from the simulation trajectory, is shown in Figure 5a. Before the negatively charged ssDNA was driven into the nanopore, the motion of the ssDNA was diffusive, and the free end of the ssDNA was in and out of the nanopore four times, evidenced by four dips (at around 8, 11, 14, and 16 ns) in Figure 5a. At around 18 ns, a larger dip (more negatively charged) indicates that the ssDNA was transiting the pore. After that, the drug-like molecule along with the protein was transiently trapped at the pore entrance, during which values of q_{eff} fluctuated because of the flexible drug−ssDNA complex. Correspondingly, the electric driving force F_e ($=q_{eff}E$) also fluctuated. Followed by another dip (close to 20 ns) when $q'_{eff} = -4.8e$ and the instant electric driving force was maximal, a rupture event occurred. After the drug-like molecule moved through the pore, q_{eff} became zero.

When V_{cr} = 2 V, Figure 4b shows that the critical electric field E_{cr} inside of the pore is approximately 0.5 V/nm. Therefore, the estimated rupture force F_e ($=q'_{eff}E_{cr}$) of the

DOI: 10.1021/jz5025614
J. Phys. Chem. Lett. 2015, 6, 331−337

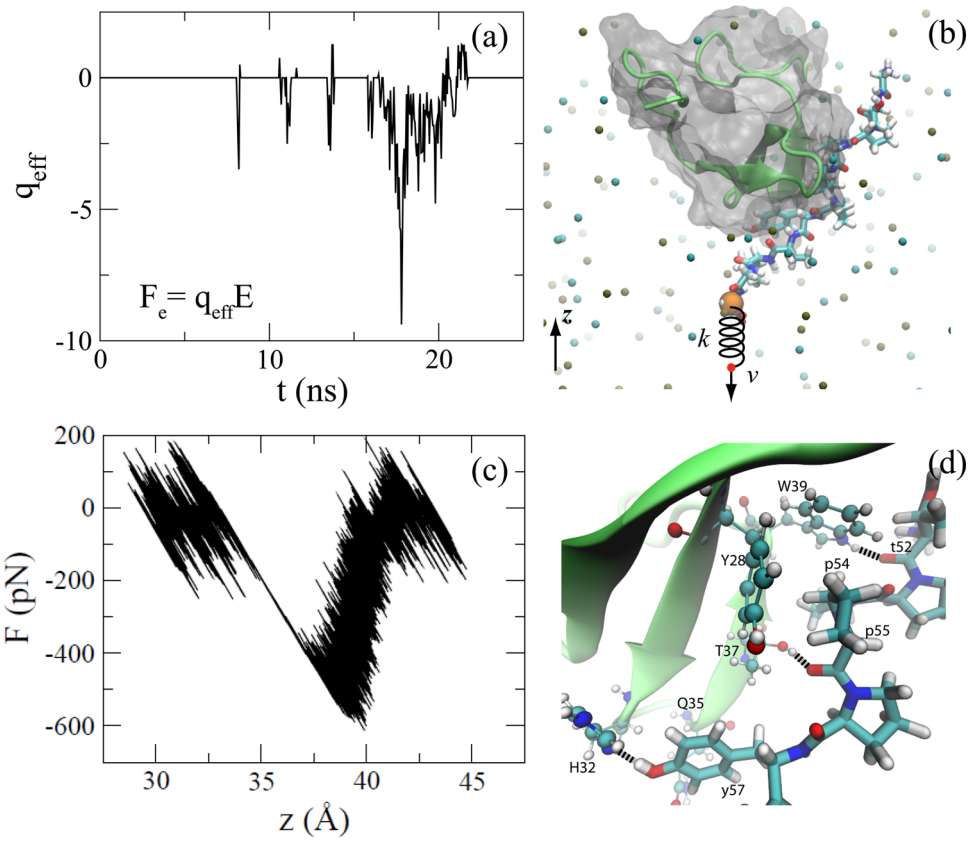

Figure 5. Mechanics in the process of pulling the drug-like molecule apart from the target protein. (a) The calculated effective charge of the drug–ssDNA fragment that is inside of the nanopore (from the MD trajectory when V_{bias} = 2 V). The mean electric driving force is $q_{eff}E$. (b) The setup of the steered molecular dynamics (SMD) simulation for mechanically pulling the drug-like molecule (shown in "stick" representation) apart from the protein (shown in both cartoon and molecular surface representations). Pulled by a harmonic spring (k = 100 pN/Å) moving at the constant velocity (v = 1 Å/ns), the C_α carbon atom at the end of the drug-like molecule is highlighted as an orange sphere. K^+ and Cl^- are shown as tan and cyan dots. (c) Force–position dependency during the rupture process. (d) The illustration of interactions between the protein and the drug-like molecule, right before the separation.

complex is 384 pN. Assuming that the potential well for the bound complex is harmonic and the bonds (such as hydrogen bonds) break after being stretched by d = 2 Å, the binding energy of the complex after integration is estimated as $F_e d/2$, that is, 5.54 kcal/mol. The more accurate binding affinity can be obtained by theoretically fitting the experimentally measured mean lifetime (see below) of the complex in external biasing fields.

Note that V_{cr} obtained from the simulation provides an upper bound, and the rupture may occur at an even lower V_{bias} at a time scale much larger than that in simulation (such as milliseconds or seconds in experiment). Theoretically, the kinetics for the rupture process can be described by the survival probability $S(t)$[36] that satisfies the first-order rate equation $dS(t)/dt = -S(t)/\tau(V_{bias})$. Here, $S(t=0) = 1$, and $\tau(V_{bias})$ is the mean lifetime of the complex with the applied biasing voltage V_{bias}. Thus, $S(t) = e^{-t/\tau(V_{bias})}$, which shows that $S(t)$ exponentially decays with the time. From the Bell relation,[37] the time to transit a tilted energy barrier due to an external biasing field can be formulated as $\tau(V_{bias}) = \tau_0 e^{-q_{eff}Ez'/k_BT}$, where k_B is the Boltzmann constant, T is the absolute temperature, τ_0 can be determined using the Kramer's theory, and z' is the distance from the potential well (an initial state) to the potential barrier (an transition state). Thus, when reducing V_{bias} (or E) in simulation, the mean lifetime of the complex increases exponentially. Within the reasonable simulation time scale (typically hundreds of nanoseconds to microseconds), the survival probability of the complex can be close to 1 for low biasing voltages. Therefore, when statistically sampling the rupture process at a larger time scale (such as in experiment) is possible, V_{cr} could be less than the one obtained from MD simulations.

For example, if τ_{exp} and τ_{sim} respectively denote the mean lifetimes for the complex in experiment (with a low biasing voltage V_{exp}) and that in simulation (with a high biasing voltage V_{sim}), from the relation given above, one can obtain $\ln(\tau_{exp}) - \ln(\tau_{sim}) = -q_{eff}(V_{exp} - V_{sim})z'/D/k_BT$. Here, $z' = d$, D (= 3 nm) is the thickness of the pore, q_{eff} = 4.8 e, V_{sim} = 2 V, and T = 300 K. In simulation, τ_{sim} (at 2 V of the voltage biasing) is about 10 ns. If τ_{exp} measured in experiment is about 1 ms, V_{exp} = 1.1 V, which is about two times smaller than V_{sim}.

To further verify the mechanics for the electric rupture of the complex, we performed the steered molecular dynamics (SMD) simulations, as illustrated in Figure 5b. In the SMD simulation, the complex was oriented the same as the one trapped inside of the pore. During the simulation, the backbone of the target protein was restrained, and the C_α carbon atom at one end of the drug-like molecule was pulled along the $-z$ direction. In the SMD simulation, one end of the spring (k = 100 pN/Å) was attached to the C_α carbon atom, while the other end of the spring was attached to a stage that moved at a constant velocity v (1 Å/ns).

DOI: 10.1021/jz5025614
J. Phys. Chem. Lett. 2015, 6, 331–337

Figure 5c shows the dependence of forces (in the pulling spring) on the positions of C_α. The position of the C_α (z) started at around 43 Å and barely changed at the beginning. Thus, the force in the spring built up and eventually was larger than the rupture force. After the rupture ($z \approx 38$ Å), the C_α atom moved forward quickly to about 34 Å (Figure 5c), catching up with the pulling stage. Meanwhile, the tensile force in the spring decreased substantially to near zero. From this simulated rupture process, the rupture force was around 488 pN. This value is comparable to the estimation (384 pN) from the electric rupture, confirming that it is reasonable to obtain the rupture force from the electric pulling process inside of the nanopore. The somewhat larger mechanical rupture force from the SMD simulation may result from the fast pulling process (1 Å/ns). Generally, the measured force becomes smaller when decreasing the pulling velocity (or the loading rate of the pulling force) in the SMD simulation.

The atomic view of the complex right before the rupture process is illustrated in Figure 5d. Besides the hydrophobic interaction between the drug-like molecule (such as residues p54 and p55, residue name lower-cased for the drug-like molecule) and the target protein (such as residues Y28, T37, and W39, residue name upper-cased for the target protein), there exist three hydrogen bonds, between W39 and p52, T37 and p55, and H32 and y57, respectively (see Figure 5d). The first two hydrogen bonds are also present in the crystal structure[38] of the complex. During the rupture process (see the movie in Supporting Information), all hydrogen bonds and hydrophobic interactions broke nearly simultaneously, which accounts for the large rupture force (488 pN).

To further demonstrate the feasibility of the nanopore-based sensor for lead optimization, we mutated the residue y57 in the drug-like molecule into a57. As shown above, the residue y57 plays an important role in the binding. It is expected that after the mutation, the rupture event inside of the nanopore should occur at a lower biasing voltage. Figure S2 in the Supporting Information shows that in independent MD simulations, after the mutation, the rupture between the drug-like molecule and the protein happens when the biasing voltage is only 1 V. Thus, these additional MD simulations indicate that the binding affinity can be estimated from the critical biasing voltage.

Our current case study demonstrates that it is possible to apply the NFS to evaluate the drug molecules prescreened or designed for a target protein. From the MD simulations, the entire screening process can be summarized as below. Initially, at a low biasing voltage, when there is no current signal as shown in Figure 1b, the complex is not trapped inside of the pore. This indicates weak or no binding between the target protein and a tested drug molecule. Therefore, tested drug molecules transit the nanopore along with the ssDNA (without being trapped), showing temporary dips in the ion current. After achieving the trapping of several different kinds of complexes, further lead optimization can be carried out by ramping up the biasing voltage to obtain the V_{cr}. A rupture event can be discerned when the ion current increases from a blockage level to the open-pore value when $V_{bias} = V_{cr}$. From many different rupture events, a distribution of V_{cr} can be obtained where the mean value determines the interaction strength between a drug molecule and the target protein. Note that the rate of voltage ramping can affect the measured values of V_{cr} because it determines the waiting time at each biasing voltage and consequently affects the survival probability of the complex (see the discussion above). The same protocol can be applied to off-target tests for a drug candidate to ensure the selectivity of the potential drug.

In summary, we have proposed a nanopore-based sensor for screening drug molecules for a target protein. A sample preparation is required to chemically link a drug candidate to an ssDNA fragment, so that the drug molecule or the complex after the binding can be electrophoretically driven toward the nanopore. It may also be convenient to replace the charged ssDNA molecule with a charged peptide (such as the aspartate-rich one). The size of a target protein should be known prior to experiment, so that nanopores with diameters less than that of the protein can be prepared. With recent development of the nanopore technology, small pores (such as 2 nm in diameter) can be achieved in a thin solid membrane.[39] The binding strength between a drug molecule and a target protein can be derived from rupture events (signified by ion currents) at applied V_{cr}. Because each transport/rupture event typically lasts for about a millisecond or less[40,41] because of a short ssDNA oligomer and all analyses of electric signals can be automated, we expect that the nanopore-based drug optimization could be a promising high-efficacy, low-cost, and reliable method.

■ ASSOCIATED CONTENT

Supporting Information

Figure S1 showing the molecular structure of a drug-like molecule linked to a ssDNA fragment; Figure S2 showing the simulation system for the mutated drug molecule and the transport of the molecule at different biasing voltages; a movie showing the MD trajectory of the rupture of the complex when transiting the solid-state nanopore (V = 2 V). This material is available free of charge via the Internet at http://pubs.acs.org.

■ AUTHOR INFORMATION

Corresponding Authors

*E-mail: bluan@us.ibm.com (B.L.).
*E-mail: ruhongz@us.ibm.com (R.Z.).

Notes

The authors declare no competing financial interest.

■ REFERENCES

(1) Macarron, R.; Banks, M. N.; Bojanic, D.; Burns, D. J.; Cirovic, D. A.; Garyantes, T.; Green, D. V.; Hertzberg, R. P.; Janzen, W. P.; Paslay, J. W.; et al. Impact of high-throughput screening in biomedical research. *Nat. Rev. Drug Discovery* **2011**, *10*, 188−195.

(2) Hulme, E. C.; Trevethick, M. A. Ligand binding assays at equilibrium: validation and interpretation. *Br. J. Pharmacol.* **2010**, *161*, 1219−1237.

(3) Sigurskjold, B. W. Exact analysis of competition ligand binding by displacement isothermal titration calorimetry. *Anal. Biochem.* **2000**, *277*, 260−266.

(4) Velazquez-Campoy, A.; Freire, E. Isothermal titration calorimetry to determine association constants for high-affinity ligands. *Nat. Protoc.* **2006**, *1*, 186−191.

(5) Brandts, J. F.; Lin, L. N. Study of strong to ultratight protein interactions using differential scanning calorimetry. *Biochemistry* **1990**, *29*, 6927−6940.

(6) Morelock, M.; Ingraham, R.; Betageri, R.; Jakes, S. Determination of receptor−ligand kinetic and equilibrium binding constants using surface plasmon resonance: application to the *lck* SH2 domain and phosphotyrosyl peptides. *J. Med. Chem.* **1995**, *38*, 1309−1318.

(7) Hüsecken, K.; Hinsberger, S.; Elgaher, W. A.; Haupenthal, J.; Hartmann, R. W. Surface plasmon resonance—more than a screening technology: insights in the binding mode of σ70: core RNAP inhibitors. *Future Med. Chem.* **2014**, *6*, 1551−1565.

DOI: 10.1021/jz5025614
J. Phys. Chem. Lett. 2015, 6, 331−337

(8) Angulo, J.; Enríquez-Navas, P. M.; Nieto, P. M. Ligand−receptor binding affinities from saturation transfer difference (STD) NMR spectroscopy: the binding isotherm of STD initial growth rates. *Chem.—Eur. J.* **2010**, *16*, 7803−7812.
(9) Kasianowicz, J. J.; Brandin, E.; Branton, D.; Deamer, D. W. Characterization of individual polynucleotide molecules using a membrane channel. *Proc. Natl. Acad. Sci. U.S.A.* **1996**, *93*, 13770−13773.
(10) Branton, D.; Deamer, D.; Marziali, A.; Bayley, H.; Benner, S.; Butler, T.; Di Ventra, M.; Garaj, S.; Hibbs, A.; Huang, X.; et al. The potential and challenges of nanopore sequencing. *Nat. Biotechnol.* **2008**, *26*, 1146−1153.
(11) Dekker, C. Solid-state nanopores. *Nat. Nanotechnol.* **2007**, *2*, 209−215.
(12) Palyulin, V. V.; Ala-Nissila, T.; Metzler, R. Polymer translocation: the first two decades and the recent diversification. *Soft Matter* **2014**, *10*, 9016−9037.
(13) Yusko, E.; Johnson, J.; Majd, S.; Prangkio, P.; Rollings, R.; Li, J.; Yang, J.; Mayer, M. Controlling protein translocation through nanopores with bio-inspired fluid walls. *Nat. Nanotechnol.* **2011**, *6*, 253−260.
(14) Plesa, C.; Kowalczyk, S. W.; Zinsmeester, R.; Grosberg, A. Y.; Rabin, Y.; Dekker, C. Fast translocation of proteins through solid state nanopores. *Nano Lett.* **2013**, *13*, 658−663.
(15) Hornblower, B.; Coombs, A.; Whitaker, R.; Kolomeisky, A.; Picone, S.; Meller, A.; Akeson, M. Single-molecule analysis of DNA−protein complexes using nanopores. *Nat. Methods* **2007**, *4*, 315−317.
(16) Zhao, Q.; Sigalov, G.; Dimitrov, V.; Dorvel, B.; Mirsaidov, U.; Sligar, S.; Aksimentiev, A.; Timp, G. Detecting SNPs using a synthetic nanopore. *Nano Lett.* **2007**, *7*, 1680−1685.
(17) Tabard-Cossa, V.; Wiggin, M.; Trivedi, D.; Jetha, N. N.; Dwyer, J. R.; Marziali, A. Single-molecule bonds characterized by solid-state nanopore force spectroscopy. *ACS Nano* **2009**, *3*, 3009−3014.
(18) Hall, A.; Scott, A.; Rotem, D.; Mehta, K.; Bayley, H.; Dekker, C. Hybrid pore formation by directed insertion of α-haemolysin into solid-state nanopores. *Nat. Nanotechnol.* **2010**, *5*, 874−877.
(19) Zhou, R.; Huang, X.; Margulis, C.; Berne, B. Hydrophobic collapse in multidomain protein folding. *Science* **2004**, *305*, 1605.
(20) Liu, P.; Huang, X.; Zhou, R.; Berne, B. Observation of a dewetting transition in the collapse of the melittin tetramer. *Nature* **2005**, *437*, 159−162.
(21) Stirnemann, G.; Kang, S.-g.; Zhou, R.; Berne, B. J. How force unfolding differs from chemical denaturation. *Proc. Natl. Acad. Sci. U.S.A.* **2014**, *111*, 3413−3418.
(22) Luan, B.; Aksimentiev, A. DNA attraction in monovalent and divalent electrolytes. *J. Am. Chem. Soc.* **2008**, *130*, 15754−15755.
(23) Luan, B.; Robbins, M. O. The breakdown of continuum models for mechanical contacts. *Nature* **2005**, *435*, 929−932.
(24) Li, J.; Gong, X.; Lu, H.; Li, D.; Fang, H.; Zhou, R. Electrostatic gating of a nanometer water channel. *Proc. Natl. Acad. Sci. U.S.A.* **2007**, *104*, 3687−3692.
(25) Tu, Y.; Xiu, P.; Wan, R.; Hu, J.; Zhou, R.; Fang, H. Water-mediated signal multiplication with Y-shaped carbon nanotubes. *Proc. Natl. Acad. Sci. U.S.A.* **2009**, *106*, 18120−18124.
(26) Tu, Y.; Lv, M.; Xiu, P.; Huynh, T.; Zhang, M.; Castelli, M.; Liu, Z.; Huang, Q.; Fan, C.; Fang, H.; Zhou, R. Destructive extraction of phospholipids from Escherichia coli membranes by graphene nanosheets. *Nat. Nanotechnol.* **2013**, *8*, 594−601.
(27) Phillips, J. C.; et al. Scalable molecular dynamics with NAMD. *J. Comput. Chem.* **2005**, *26*, 1781.
(28) Jorgensen, W. L.; Chandrasekhar, J.; Madura, J. D.; Impey, R. W.; Klein, M. L. Comparison of simple potential functions for simulating liquid water. *J. Chem. Phys.* **1983**, *79*, 926−935.
(29) Neria, E.; Fischer, S.; Karplus, M. Simulation of activation free energies in molecular systems. *J. Chem. Phys.* **1996**, *105*, 1902.
(30) Beglov, D.; Roux, B. Finite representation of an infinite bulk system: solvent boundary potential for computer simulations. *J. Chem. Phys.* **1994**, *100*, 9050−9063.
(31) Cruz-Chu, E. R.; Aksimentiev, A.; Schulten, K. Water−silica force field for simulating nanodevices. *J. Phys. Chem. B* **2006**, *110*, 21497−21508.
(32) MacKerell, A., Jr.; et al. All-atom empirical potential for molecular modeling and dynamics studies of proteins. *J. Phys. Chem. B* **1998**, *102*, 3586−3616.
(33) Luan, B.; Zhou, R. Nanopore-based sensors for detecting toxicity of a carbon nanotube to proteins. *J. Phys. Chem. Lett.* **2012**, *3*, 2337−2341.
(34) Aksimentiev, A.; Schulten, K. Imaging α-hemolysin with molecular dynamics: ionic conductance, osmotic permeability and the electrostatic potential map. *Biophys. J.* **2005**, *88*, 3745−3761.
(35) Luan, B. Q.; Aksimentiev, A. Electro-osmotic screening of the DNA charge in a nanopore. *Phys. Rev. E* **2008**, *78*, 021912.
(36) Dudko, O. K.; Mathé, J.; Szabo, A.; Meller, A.; Hummer, G. Extracting kinetics from single-molecule force spectroscopy: nanopore unzipping of DNA hairpins. *Biophys. J.* **2007**, *92*, 4188−4195.
(37) Bell, G. I. Models for the specific adhesion of cells to cells. *Science* **1978**, *200*, 618−627.
(38) Pires, J. R.; Taha-Nejad, F.; Toepert, F.; Ast, T.; Hoffmüller, U.; Schneider-Mergener, J.; Kühne, R.; Macias, M. J.; Oschkinat, H. Solution structures of the YAP65 WW domain and the variant L30 K in complex with the peptides GTPPPPYTVG, N-(n-octyl)-GPPPY and PLPPY and the application of peptide libraries reveal a minimal binding epitope. *J. Mol. Bio.* **2001**, *314*, 1147−1156.
(39) Briggs, K.; Kwok, H.; Tabard-Cossa, V. Automated Fabrication of 2-nm solid-state nanopores for nucleic acid analysis. *Small* **2014**, *10*, 2077−2086.
(40) Meller, A.; Nivon, L.; Brandin, E.; Golovchenko, J.; Branton, D. Rapid nanopore discrimination between single polynucleotide molecules. *Proc. Natl. Acad. Sci. U.S.A.* **2000**, *97*, 1079−1084.
(41) Storm, A. J.; Storm, C.; Chen, J.; Zandbergen, H.; Joanny, J.-F.; Dekker, C. Fast DNA translocation through a solid-state nanopore. *Nano Lett.* **2005**, *5*, 1193−1197.

DOI: 10.1021/jz5025614
J. Phys. Chem. Lett. 2015, 6, 331−337